ResearchGate

See discussions, stats, and author profiles for this publication at: https://www.researchgate.net/publication/45404904

Polarization Dependence of Holographic Grating Recording in Azobenzene-Functionalized Polymers Monitored by Visible and Infrared Light

ARTICLE *in* THE JOURNAL OF PHYSICAL CHEMISTRY B · AUGUST 2010

Impact Factor: 3.3 · DOI: 10.1021/jp103756h · Source: PubMed

CITATIONS
36

READS
61

4 AUTHORS, INCLUDING:

Andrzej Miniewicz
Wroclaw University of Technology
223 PUBLICATIONS **1,848** CITATIONS
SEE PROFILE

Ewa Schab-Balcerzak
Polish Academy of Sciences
114 PUBLICATIONS **872** CITATIONS
SEE PROFILE

Available from: Andrzej Miniewicz
Retrieved on: 27 January 2016

Polarization Dependence of Holographic Grating Recording in Azobenzene-Functionalized Polymers Monitored by Visible and Infrared Light

Anna Sobolewska,*,† Stanislaw Bartkiewicz,† Andrzej Miniewicz,† and Ewa Schab-Balcerzak‡

Institute of Physical and Theoretical Chemistry, Wroclaw University of Technology, Wybrzeze Wyspianskiego 27, 50-370 Wroclaw, Poland, and Centre of Polymer and Carbon Materials, Polish Academy of Sciences, M. Curie-Sklodowska 34, 41-819 Zabrze, Poland

Received: April 26, 2010; Revised Manuscript Received: June 9, 2010

The holographic grating recording process in thin films of amorphous azobenzene-functionalized polymers has been widely reported in the literature. In spite of the many reports, little is known about the mechanisms responsible for different temporal behaviors of the diffraction efficiency during long recording times. Here, we report on experimental studies of the diffraction efficiency changes during the holographic diffraction grating recording process in photochromic polymer. The gratings were inscribed for four different polarization combinations of the recording beams: *s-s*, *p-p*, *s-p* and right to left circular polarization (*RCP-LCP*) employing the degenerate two-wave mixing technique. The grating recording process was simultaneously monitored by three different wavelengths: 514.5 nm (writing) and 632.8 and 904 nm (reading). The temporal evolution of the diffraction efficiency (for all polarization configurations and for each wavelengths) was precisely fitted within the model, which assumes simultaneous formation of the absorption grating and three coupling phase gratings shifted by 0 or π with respect to each other. Two of the phase gratings originate from the refractive index grating changes in the bulk (volume) of a material and the third one from the surface relief modulation. The model enabled us to extract relevant parameters for each grating such as the build-up time constant, its final amplitude, and the phase shifts between phase gratings. Performed studies and the discussion of results revealed the main differences in the diffraction grating formation process for *s-s*, *p-p*, *s-p*, and *RCP-LCP* polarization configurations.

1. Introduction

Azobenzene-functionalized polymers belong to a class of holographic materials extensively investigated in the past decade because of their possible application in optical information storage and processing,[1−3] polarization holography,[4,5] and photonics.[2,6−13] These applications rely on photoinduced optical anisotropy (POA)[2,4,14−16] and surface relief grating (SRG) formation[2,4,14,17−20] occurring simultaneously in amorphous thin films of azobenzene-functionalized polymers when they are irradiated by two interfering polarized laser beams.[2,21,22] The dynamics and the strength of POA and SRG can be measured by observation of the first order diffraction efficiency dynamics (DED) during the holographic grating recording process, which can be realized either in a degenerate two-wave mixing (DTWM) experiment or its version using the Lloyd mirror.[23]

Many papers have reported on DED of the holographic grating inscription process in different azobenzene-functionalized polymers,[2,21−24] its dependence on the polarization of the writing beams,[2,18,21,22,24−28] SRG characterization,[2,22−24,27,29,30] and mechanisms of the SRG formation,[2,25,30−37] whereas only a few deal with the mechanism explaining the DED.[21,22,38−42] The first papers devoted to mechanisms explaining the DED assumed the formation of only two phase gratings, the bulk refractive index grating and the SRG, while the absorption grating was usually neglected in order to simplify the explanation.[21,22,38] Such assumptions are sufficient to explain the simple exponential behavior of the DED, but they do not explain the complex (nonexponential) DED frequently observed by us[43,44] and other research groups.[2,21−25,33]

We have focused our attention on finding the explanation of the complex DED in azo-polymers.[40−42] On the basis of observations of the holographic grating recording experiments and the paper written by Reinke et al.,[39] we additionally assumed, beside the formation of two phase gratings (the bulk refractive index grating and a surface relief one), the time-dependent phase shift between them.[40] On the basis of these assumptions and using the simple model of the vectorial grating approach, a series of numerical simulations were performed. They revealed both the simple and the complex DED in azo-polymers.[40] The assumption about the time-dependent phase shift between the bulk and the surface gratings requires a symmetry breaking during the holographic grating recording process (it was discussed in detail in ref 40). There is a question of how the nonexponential DED can be explained when the symmetry during the grating inscription process is not broken.

In order to investigate this problem, experiments in which special attention was paid to preserve the symmetry during the grating recording process (in order to exclude the symmetry breaking conditions) were performed,[41] resulting again in complex temporal behaviors of the diffraction efficiency. In order to explain the DED, we followed the new idea that assumes simultaneous formation of three phase gratings during the grating recording process. The idea comes from the results of the time-resolved X-ray and visible light scattering experiments performed during the SRG formation process in azobenzene side-chain polymer film.[45] Assuming the formation of three phase gratings (two of them arise in the bulk of the polymer

* To whom correspondence should be addressed. Telephone: (048) 71-320-23-17; fax: (048) 71-320-33-64; e-mail: anna.sobolewska@pwr.wroc.pl.
† Wroclaw University of Technology.
‡ Polish Academy of Sciences.

10.1021/jp103756h © 2010 American Chemical Society
Published on Web 07/13/2010

film and the third one arises at the surface) with different build-up time constants and constant (equal to 0 or π) phase shifts between them and applying the model of vectorial grating approach, we were able to explain the complex DED.[41,42] The presence of absorption grating was also taken into account.

In this work we report on holographic grating inscription using four different polarization configurations of the recording beams: *s-s*, *p-p*, *s-p* (*s* and *p* denote the light polarized perpendicular and parallel to the incidence plane, respectively), and right and left circular polarizations (*RCP-LCP*) together with the model explaining different temporal behaviors of the diffraction efficiency. The grating recording process was simultaneously monitored by three different wavelengths: 514.5 nm (writing) and 632.8 and 904 nm (reading). The DED curves for all polarization configurations and all wavelengths are consistently described within the model assuming simultaneous formation of three phase gratings, with constant phase shifts (0 or π) between them, and the absorption grating. The model enables extraction of the information about the grating recording time constants, the grating amplitudes, and the phase shifts between the phase gratings from the measured DEDs. This allowed us to look deeply into the diffraction grating recording process and to make a comparison of the grating inscription process for different polarization configurations for the same material.

A mechanism assuming the formation of three phase gratings and the absorption grating was recently developed by us in order to explain the complex DED obtained for the significantly long recording time of the holographic grating inscription in azo-polymers.[42]

In contrast to rare reports on the mechanisms explaining different temporal behaviors of the diffraction efficiency during the holographic gratings process in azo-polymers, the polarization dependency of the formation of the SRGs has been widely investigated by different research groups. Tripathy and co-workers performed a detailed analysis of the influence of the polarization configuration of the writing beams on the amplitude of the surface modulation.[2,24−26] They applied seven different polarization geometries.[2,25] Lagugne-Labarthet et al. investigated the light diffraction efficiency, birefringence, and surface modulation induced by linearly polarized beams, a combination of ±45° and circularly polarized beams and co- and contracircularly polarized beams.[21−23] We also reported on the polarization dependence of light DED and the surface relief modulation for three different linear polarization combinations of the writing beams.[27] Detailed studies on the polarization dependence of the formation of SRGs (seven polarization geometries) were also performed in azobenzene-containing molecular glasses.[28] In most of these studies, different DEDs (simple exponential and the complex nonexponential) were observed for different polarization configurations used for the grating inscription process with no microscopic explanation of their behavior.[2,21−25,27,28]

2. Experimental Section

Materials. Newly synthesized poly(amido-imide) (PAI) containing two azobenzene moieties as the side groups was used in reported studies. PAI chemical structure and absorption spectra are shown in Figure 1. The polymer molecular weight (M_w) and number-average molecular weight (M_n) (relative to polystyrene standards) were 14.90×10^3 and 10.3×10^3, respectively, and polydispersity was 1.45. The glass transition temperature was not observed by DSC up to 300 °C. The synthesis procedure and the polymer characterization can be found elsewhere.[46] The polymer film was prepared by casting

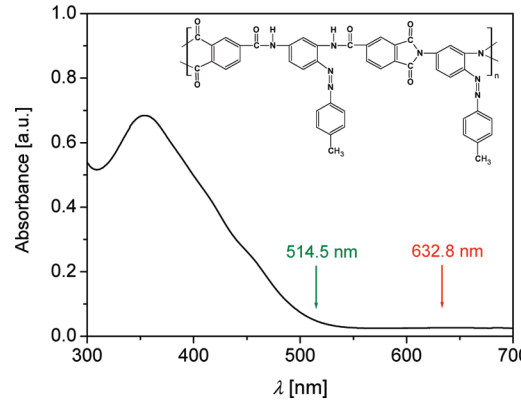

Figure 1. PAI absorption spectrum (as a film cast on a microscopic glass plate) and its chemical structure. The arrows indicate the position of the 514.5 and 632.8 nm lines used in writing and monitoring, respectively (904 nm is outside the scale).

the solution of PAI in *N*-methyl-2-pyrrolidone onto the clean glass microscope slide. The film was dried in temperature 100 °C during 5 h and then in 200 °C during 1 h in a vacuum. The polymer film thickness (d_0) was determined with an interference microscope (Tolansky method) ranging from 1.39 to 1.58 μm.

Holographic Setup. Holographic grating recording was performed using a standard DTWM technique. The experimental setup of DTWM is depicted in Figure 2.

The gratings were inscribed with the green line ($\lambda_1 = 514.5$ nm) of an argon ion laser (GL). The recording beam intensities were set equal $I_1 = I_2 = 560$ mW/cm^2, and the exposure time was 50 min. The angle between the writing beams was fixed at $\theta = 24°$ resulting in a grating period of $\Lambda \cong 1.24$ μm (according to $\Lambda = \lambda/2 \sin(\theta/2)$). The multiple-order light self-diffraction was observed as expected for a Raman−Nath light scattering regime. The grating build-up was simultaneously monitored by two low-power, linearly polarized, probe beams delivered from a He−Ne laser (RL, $\lambda_2 = 632.8$ nm, *s*-polarized) and from an IR laser diode (IL, $\lambda_3 = 904$ nm, *s*-polarized). The powers of Ar^+, He−Ne, and IR laser light diffracted on the grating into the first-order of diffraction were measured simultaneously as a function of time by calibrated silicon detectors (cf. Figure 2). The measured power allowed determination of the DED ($\eta(t)$).

Four qualitatively different combinations of the writing beams polarizations were used for the grating inscription: *s-s*, *p-p*, *s-p*, and *RCP-LCP*. The beam polarizations were adjusted with the help of the half-wave and the quarter-wave retardation plates.

All studied polarization geometries together with the incident light polarization modulations along the grating period Λ are shown in Table 1. In the case of *s-s* polarization geometry the resulting electric field of the optical waves oscillates along the *y*-direction ($\vec{E} \parallel y$), i.e., perpendicularly to the grating wave-vector, whereas for the *p-p* one it oscillates along the *x*-direction ($\vec{E} \parallel x$), i.e., along the grating wave-vector. There is a light intensity modulation along the *x*-direction for *s-s* and *p-p* configurations. In the mutually orthogonal linear polarization, *s-p* geometry, the intensity of the light is constant along the grating wave-vector, but the resultant polarization states are varying between linear, elliptical, and circular ones as it is shown in Table 1. For the two opposite circularly polarized beams (*RCP-LCP*) the intensity of the light is also constant, but the resulting electric filed of the optical waves is always linear, and its direction is rotating along the period. The full Jones matrix description of these configurations has been given in ref 22.

AFM Measurements. The topography of the polymer surface at the illuminated area was examined by an atomic force

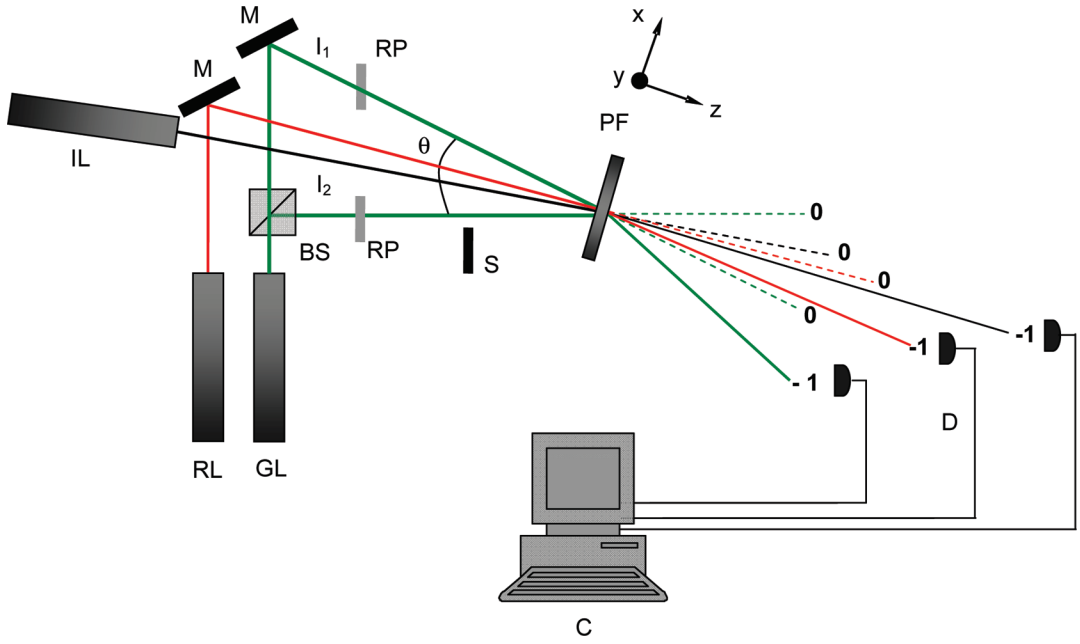

Figure 2. DTWM experimental setup: GL, RL, and IL - lasers emitting green ($\lambda_1 = 514.5$ nm), red ($\lambda_2 = 632.8$ nm), and infrared ($\lambda_3 = 904$ nm) light, respectively; BS - beam splitter, M - mirror, RP - retardation plate ($\lambda/2$, $\lambda/4$), S - shutter, PF - polymer film, D - detector, C - computer.

TABLE 1: Periodic Polarization Modulation of the Light Used for the Grating Inscription for Different Polarization Geometries: *s-s*, *p-p*, *s-p*, and *RCP-LCP*[a]

Position (x)	0	$\Lambda/8$	$\Lambda/4$	$3\Lambda/8$	$\Lambda/2$	$5\Lambda/8$	$3\Lambda/4$	$7\Lambda/8$	Λ	Light intensity in the film plane (x,y)
s-(-s)	·	↕	↕	↕	↕	↕	↕	↕	·	$2I\sin^2\left(\frac{\delta}{2}\right)$
p-p	↔	↔	↔	↔	·	↔	↔	↔	↔	$2I\cos^2\left(\frac{\delta}{2}\right)$
s-p	↗	↺	○	↻	↘	↻	○	↺	↗	I
RCP-LCP	↔	↙	↗	↕	↕	↖	↘	↙	↔	I

[a] The polarization states are given according to the reference axes (x,y) and are reported as a function of the phase difference (δ) between the two interfering pump beams along the grating wave-vector. Here I is a sum of light intensities of the interfering beams.[22]

microscopy technique, using a Dimension V Scanning Probe Microscope by Veeco and working in tapping mode.

3. Theoretical Approach

Irradiation of amorphous azo-functionalized polymer film by two interfering polarized laser beams induces a spatially modulated optical anisotropy in the bulk of a material, i.e., changes of the refractive index (Δn) and the absorption coefficient ($\Delta\kappa$). These changes are accompanied by a periodic surface corrugation (Δd), defined as an SRG, of the freestanding side of a film deposited on a glass substrate. The power of light diffracting on the grating into the first order of diffraction serves as a measure of temporal evolution of the grating build-up process and is a function of the induced material anisotropy, the surface relief modulation depth, and the light wavelength.

The ratio of the intensities of the first-order diffracted beam ($I_{1,\mathrm{diff}}$) and the incident beam (I_{inc}) defines the diffraction efficiency $\eta = I_{1,\mathrm{diff}}/I_{\mathrm{inc}}$. It has two components resulting from the light diffraction on the phase (η_p) and the absorption (η_a) gratings:

$$\eta(t) = \eta_p(t) + \eta_a(t) \tag{1}$$

For the thin sinusoidal gratings, the diffraction efficiency of the phase grating $\eta_p(t)$ is described by the square of the first-order Bessel function $J_1(\Phi)$,[47] and the diffraction efficiency of the absorption grating $\eta_a(t)$ can be expressed by the square of the sinusoidal function (for the small changes of the absorption coefficient):[42]

$$\eta(t) = J_1^2[\Phi(t)] + \sin^2[\Phi_a(t)] \tag{2}$$

where $\Phi(t)$ and $\Phi_a(t)$ are arguments of the phase and amplitude gratings, respectively.

The phase grating can be deconvoluted into three gratings. In order to also include the mutual phase shifts between these gratings, the vectorial grating approach has to be applied for the proper description of $\Phi(t)$ defined as the optical retardation between grating extremes:[39−42]

$$\Phi(t) = \sqrt{\Phi_1^2(t) + \Phi_2^2(t) + \Phi_3^2(t) + 2\Phi_1(t)\Phi_2(t)\cos\varphi_{12} + 2\Phi_2(t)\Phi_3(t)\cos\varphi_{23} + 2\Phi_1(t)\Phi_3(t)\cos\varphi_{13}} \quad (3)$$

where $\Phi_1(t)$, $\Phi_2(t)$ and $\Phi_3(t)$ express the temporal changes of the accumulated phase during passage of light through the respective gratings, whereas φ_{12}, φ_{23}, and φ_{13} are the phase shifts between them. We assume that each individual grating dynamics is described by the single-exponential function:

$$\Phi_i(t) = \Phi_{i,\max}[1 - \exp(-t/\tau_i)], \quad i = (1, 2, 3) \quad (4)$$

where τ_i (i = 1, 2, 3) are the recording time constants of the phase gratings formation, $\Phi_{i,\max}$ are the maximum optical retardations of phase gratings defined as:

$$\Phi_{i,\max} = \frac{2\pi\Delta n_{i,\max} d}{\lambda}, \quad i = (1, 2) \quad \text{and} \quad \Phi_{3,\max} = \frac{2\pi n_{\text{eff}}\Delta d_{\max}}{\lambda} \quad (5)$$

where $\Delta n_{i,\max}$ (i = 1,2) and $\Delta d_{\max}$ are the maximum refractive index and thickness modulations, respectively, d is the polymer film thickness, n_{eff} is the effective refractive index for a corrugated surface, $n_{\text{eff}} \approx (n_p + n_0)/2$, where n_p and n_0 denote the refractive index of polymer and air, respectively.[3]

We also assume that the volume absorption grating optical phase retardation ($\Phi_a(t)$) is described by the single-exponential function:

$$\Phi_a(t) = \Phi_{a,\max}[1 - \exp(-t/\tau_a)] \quad (6)$$

where τ_a is its recording time constant and $\Phi_{a,\max}$ is given by

$$\Phi_{a,\max} = \frac{\Delta\kappa_{\max} d}{2} \quad (7)$$

where $\Delta\kappa_{\max}$ is the maximum absorption coefficient modulation.

We propose the following origin of the three phase gratings formed during the holographic recoding process in azobenzene-functionalized polymer films.[42] The first grating (Φ_1) is connected with volume geometrical changes of the azobenzene groups, which arise from the *trans−cis−trans* photoisomerization cycles leading to their alignment and material birefringence. It is the fastest grating among the phase gratings, and we will define it as the reorientation grating. Since azobenzene derivatives are chemically attached to polymer main chains, their rearrangement affects the polymer main chains spatial reorganization. It is the origin of the second grating (Φ_2) and the third grating (Φ_3) formation, where Φ_2 is a result of the polymer mass flow in the bulk of the material, i.e., forming the volume density grating, and Φ_3 represents the polymer mass flow expressed as the surface corrugation. The third grating has the longest recording time constant. Since mass transport occurs as a result of the diffusion, we will name these two gratings as the bulk and the surface diffusion gratings. The latter one we will name alternatively as the SRG.

The source of absorption grating is linked with the molecular reorientation process due to angular hole burning and dichroism caused by photoalignment of azobenzene derivatives due to multiple *trans−cis−trans* transitions.

4. Results and Discussion

A. Experimental Results. Different combinations of the recording beam polarizations revealed the different DEDs. The experimental curves for the first-order diffracted beams for recording and monitoring beams (always s-polarized), for *s-s*, *p-p*, *s-p*, and RCP-LCP polarization geometries are gathered in Figure 3. The noise free curves of $\eta(t)$ for RL and IL are due to diffraction of the monitoring beams on the grating, whereas the noisy curve for GL corresponds to the self-diffraction process. The significant noise appearing on GL curves only arises as a result of beam coupling induced by mechanical instabilities temporarily shifting the light interference pattern with respect to the existing grating. This process leads to energy exchange between beams. Here this noise is substantial due to relatively small grating period Λ.

The maximum diffraction efficiencies and the SRG modulations are given in Table 2.

After completing the grating inscription process (at 3000 s), the illuminated area was investigated by a scanning probe microscope in order to measure the SRG grating amplitudes. From the surface topography measurements using an atomic force microscope working in tapping mode, we elucidated the respective amplitudes of SRGs for each of polarization combinations (cf. Table 2).

There is a substantial difference between light self-diffraction and diffraction processes on a refractive index grating. The diffracted intensity into first order in a self-diffraction process is given by

$$I_{\pm 1} = TI_0[J_1^2(\Phi) + J_2^2(\Phi)] \quad (8)$$

where T is the sample transmission, whereas for the diffraction process, only the first term in the square bracket of the equation above is present. Therefore different behavior is expected for the DED for GL when compared with that of RL and IR. Another source of difference is the different light polarization and absorbance for recording and monitoring light wavelengths.

***s-s* Configuration.** The results of the DED measured during the grating recoding process for GL, RL, and IL are shown in Figure 3a. The magnitude and shape of $\eta(t)$ for three wavelengths were comparable. When the pump laser (GL) was switched on, the dynamics of the diffraction efficiency exhibited a relatively fast growth. At around 500 s diffraction efficiency for GL reached a maximum $\eta_{\max}$ = 1.8%, whereas the maxima $\eta_{\max}$ for RL (2.2%) and IL (2.3%) appeared later on. For the longer times the diffraction efficiencies started to slowly decrease. The depth of the surface relief modulation $\Delta d^{s\text{-}s}$ at the end of the recording, i.e., at 3000 s, was 21 nm.

***p-p* Configuration.** The results of the DED for recording and monitoring wavelengths are gathered in Figure 3b. The DED was qualitatively different from that observed for *s-s* polarization geometry. Here, $\eta(t)$ for three wavelengths exhibits a slow, but steady increase up to the end of the recording time (3000 s). The increase rate was faster at the beginning of the recording

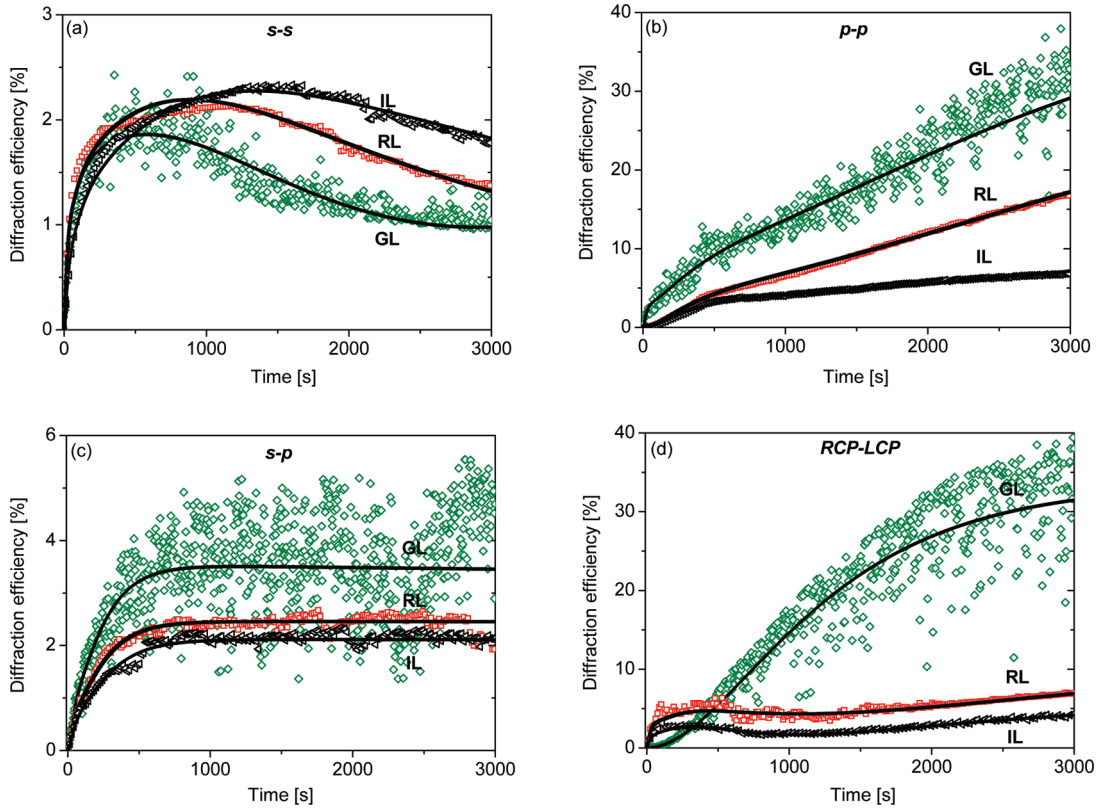

Figure 3. DED $\eta(t)$ measured during the holographic grating recording in azobenzene-functionalized polymer thin film for different polarization configurations: *s-s* (a), *p-p* (b), *s-p* (c), and *RCP-LCP* (d): experimental data (symbols) and theoretical fit (lines). In panels a−d, $\eta(t)$ for writing line GL ($\lambda_1 = 514.5$ nm) and monitoring lines RL ($\lambda_2 = 632.8$) and IL ($\lambda_3 = 904$ nm) is presented.

TABLE 2: Maximum Diffraction Efficiencies and SRG Modulation Depths Measured for *s-s*, *p-p*, *s-p*, and *RCP-LCP* Polarization Combinations of the Writing Beams in Azo-Polymer

	maximum diffraction efficiencies η_{max} [%] for wavelength λ [nm]			
polarization configuration	514.5	632.8	904	SRG modulation depth Δd [nm]
s-s	1.8	2.2	2.3	21
p-p	29.1	17.1	7.1	178
s-p	3.5	2.5	2.1	3
RCP-LCP	31.5	7.0	4.1	118

process when compared to the increase rate for the longer time. The maximum diffraction efficiency were measured after 3000 s. The highest value of η was observed for the recording wavelength $\lambda_1 = 514.5$ nm, $\eta_{514.5} = 29.1\%$, which is close to the maximum diffraction efficiency predicted by the square of the J_1 Bessel function. Relatively large diffraction efficiency was observed for the monitoring wavelengths $\eta_{632.8} = 17.1\%$ for $\lambda_2 = 632.8$ nm (RL) and $\eta_{904} = 7.1\%$ for $\lambda_3 = 904$ nm (IL), respectively. η were the highest among all studied polarization geometries (cf. Table 2). The amplitude of the SRG was the highest among all the studied polarization geometries amounting to $\Delta d^{p\text{-}p} = 178$ nm.

***s-p* Configuration.** In the case of the linear orthogonal polarizations of the recording beams, the DED was different both from *s-s* and *p-p* polarization configurations (Figure 3c). DEDs for the used wavelengths were comparable to each other. $\eta(t)$ dependence revealed an increase at the beginning of the grating recording process up to the maximum, reached after 700 s, and it stayed unchanged to the end of the recoding time. The maximum diffraction efficiencies for all wavelengths were between 2 and 4%, higher for GL and lower for IL (Table 2). The surface modulation in this case was negligible (∼3 nm).

***RCP-LCP* Configuration.** The experimental results for the *RCP-LCP* polarization geometry are shown in Figure 3d. The striking feature was that the DED for RL and IL were similar, whereas for GL $\eta(t)$ dependence was totally different. At the beginning of the grating recording process, the diffraction efficiency for RL and IL exhibited a rapid increase up to the maximum, which appeared at around 250 s. After that, the DED started to decrease, reaching the minimum, and again started to increase slowly. In the case of GL, $\eta(t)$ showed a small increase in rate at the beginning followed by faster one, which was continued up to the end of the recording process. The difference between the dynamics for writing (GL) and monitoring (RL, IL) beams resulted from their different polarization states; the writing beam was circularly polarized, whereas the monitoring beams were linearly polarized. The highest maximum diffraction efficiency was obtained for the recording beam $\lambda_1 = 514.5$ nm, $\eta_{514.5} = 31.5\%$ (close to the theoretical limit) and the lowest for IL ($\eta_{904} = 4.1\%$). The depth of the SRG $\Delta d^{RCP-LCP}$ was equal to 118 nm.

DED, diffraction efficiency, and surface relief modulation depth strongly depend on the polarization configuration of the recording beams (Figure 3, Table 2). The value of the diffraction efficiency for each polarization geometry depends on the wavelength.

DEDs for each polarization geometry were comparable when the writing and monitoring light beams exhibited the same polarization state, i.e., they were all linearly polarized. In the case of *RCP-LCP* polarization geometry, when the recording beams were circularly polarized and monitoring beams were linearly polarized, the behaviors of $\eta(t)$ for the recording and monitoring beams were completely different.

TABLE 3: Deconvolution into Single Exponential Functions (cf. Equations 2− 7) of the Experimental Diffraction Dynamics Curves Obtained for *s-s*, *p-p*, *s-p*, and *RCP-LCP* Polarization Configurations for Recording and Monitoring Wavelengths

polarization configuration		*s-s*			*p-p*			*s-p*			*RCP-LCP*		
wavelength [nm]	λ	514.5 GL	632.8 RL	904 IL	514.5 GL	632.8 RL	904 IL	514.5 GL	632.8 RL	904 IL	514.5 GL	632.8 RL	904 IL
maximum phase grating amplitudes	$\Phi_{1,max}$	0.14	0.14	0.14	0.53	0.47	0.46	0.33	0.27	0.25	0[b]	0.87	0.71
	$\Phi_{2,max}$	0.21	0.21	0.21	0.22	0.20	0.17	0[a]	0[a]	0[a]	0[b]	1.41	0.44
	$\Phi_{3,max}$	1.13	0.71	0.43	3.00	2.07	0.84	0[a]	0[a]	0[a]	1.80	1.10	0.70
phase grating recording time constants [s]	τ_1		65			250			180			250	
	τ_2		610			610			[a]			610	
	τ_3		7900			7900			[a]			7900	
phase shifts between gratings	φ_{12}		0			π			[a]			π	
	φ_{23}		π			π			[a]			0	
	φ_{13}		π			0			[a]			π	
absorption grating recording time constant [s]	τ_a		16			16			26			16	
maximum absorption grating amplitude	$\Phi_{a,max}$	0.099	0.097	0.080	0.17	0[c]	0[c]	0.095	0.082	0.076	0[b]	0.175	0.130

[a] For *s-p* polarization geometry, only Φ_1 grating dominates the response therefore τ_2, τ_3, and φ_{ij} can not be determined. [b] Can not be observed by circularly polarized light. [c] Can not be detected when the polarization of the reading beams is orthogonal to the polarization of the recording beam.

For each polarization geometry and used wavelength, the differences were observed in the maximum diffraction efficiencies (cf. Table 2). Usually the highest diffraction efficiency was measured for the recording wavelength, and the lowest one was measured for the infrared monitoring laser line, which is natural due to the refractive index dispersion and $\phi \sim 1/\lambda$. The opposite behavior has been noticed only in *s-s* polarization geometry, where the highest η was obtained for IL and the the lowest was obtained for GL.

The maximum diffraction efficiencies for the *p-p* and *RCP-LCP* polarization configurations were very high and 1 order of magnitude higher than those for *s-s* and for *s-p* geometries (Table 2). The SRG modulation was relatively deep for *p-p* and *RCP-LCP* geometries, whereas for *s-s* and *s-p* it was weak. These results are in accordance with those reported in literature, which unanimously affirmed that *p-p* and *RCP-LCP* polarization configurations, among the four studied here, are recognized as the most effective, i.e., the largest SRG amplitude and the highest diffraction efficiency are obtained, whereas *s-s* and *s-p* geometries are the least effective ones.[2,21,22,25,27] It is worth underlining that, no matter what kind of azobenzene-functionalized polymers were used and no matter what were the experimental conditions, the highest surface modulation and the highest diffraction efficiency are always measured for *p-p* and *RCP-LCP* geometries. The other issue is that there is no agreement on which of these two configurations is the most effective one. Tripathy et al. reported that *RCP-LCP* is the most effective one,[2,25] whereas Lagugne-Labarthet and co-workers obtained the best results using *p-p* geometry.[21,22] Results obtained by us seem to agree with those reported by the Lagugne-Labarthet group. There is also no agreement on which configuration is the least effective one, i.e., *s-s* or *s-p* one. According to Tripathy and co-workers,[2,25] the smallest surface relief modulation and the lowest diffraction efficiency is obtained for *s-s* geometry. This is consistent with their proposed field gradient force model, which predicts that no force acts on the polymer chains in the *s-s* configuration, and hence no appreciable SRG formation is predicted.[25,32] The results reported by Lagugne-Labarthet et al.[22] are qualitatively different because the smallest surface relief modulation was obtained for *s-p* geometry, but the lowest diffraction efficiency, was measured for *s-s* configuration (even thought the modulation depth for *s-s* was larger than for *s-p*). These conclusions are in accordance with the results reported by us previously[27] and are in agreement with the data reported here. This short, general discussion reveals how the issue of the polarization dependence of the formation of the SRGs is ambiguous, thereby it confirms how difficult is to understand the mechanisms responsible for the surface corrugation.

Summing up, in this study the largest surface relief modulation and the highest diffraction efficiency (for monitoring beams) were obtained for *p-p* polarization geometry, whereas the smallest surface modulation was obtained for *s-p* configuration, but the lowest diffraction efficiency was measured for *s-s*. These results are in a clear accordance with the Lagugne-Labarthet reports.[21,22]

B. Deconvolution of DED Curves. Assuming (*i*) simultaneous formation of three phase gratings, with constant phase shifts between them, and (*ii*) formation of the absorption grating, fitting of experimental $\eta(t)$ dependences was performed according to the described above approach. The results of the calculations are presented in Figure 3 by the solid black lines (notice that they match well the experimental curves). Fitting parameters for all studied cases are gathered in Table 3. The expected error in the experimental data is estimated to be at least 10%, and the error in determining the fitting parameters also can reach 10%.

The exemplary results of deconvolution of the dynamics of $\eta(t)$ into individual phase gratings: $\Phi_1(t)$, $\Phi_2(t)$, and $\Phi_3(t)$ for RL, described by eq 4, for each polarization configuration are shown in Figure 4I−IV(a) (cf. Table 3 for respective parameters). The dynamics of the absorption grating ($\sin^2(\Phi_a(t))$ and the dynamics of the phase grating ($J_1^2(\Phi(t))$ are presented separately in Figure 4I−IV(b) by dotted and dashed lines, respectively. In Figure 4I−IV(b) there is also shown the final DED $\eta(t)$ (solid line) as a sum of the absorption grating and the phase grating (cf. eq 2), which is also depicted in Figure 3 as a result of experimental data fitting.

As can be seen in Table 3 and Figure 4, three phase gratings with different amplitudes and recording time constants, and the absorption grating were formed for *s-s*, *p-p*, and *RCP-LCP* geometries (Figure 4I,II,IV), whereas for *s-p* (Figure 4III) only one phase grating, beside the absorption grating, was formed.

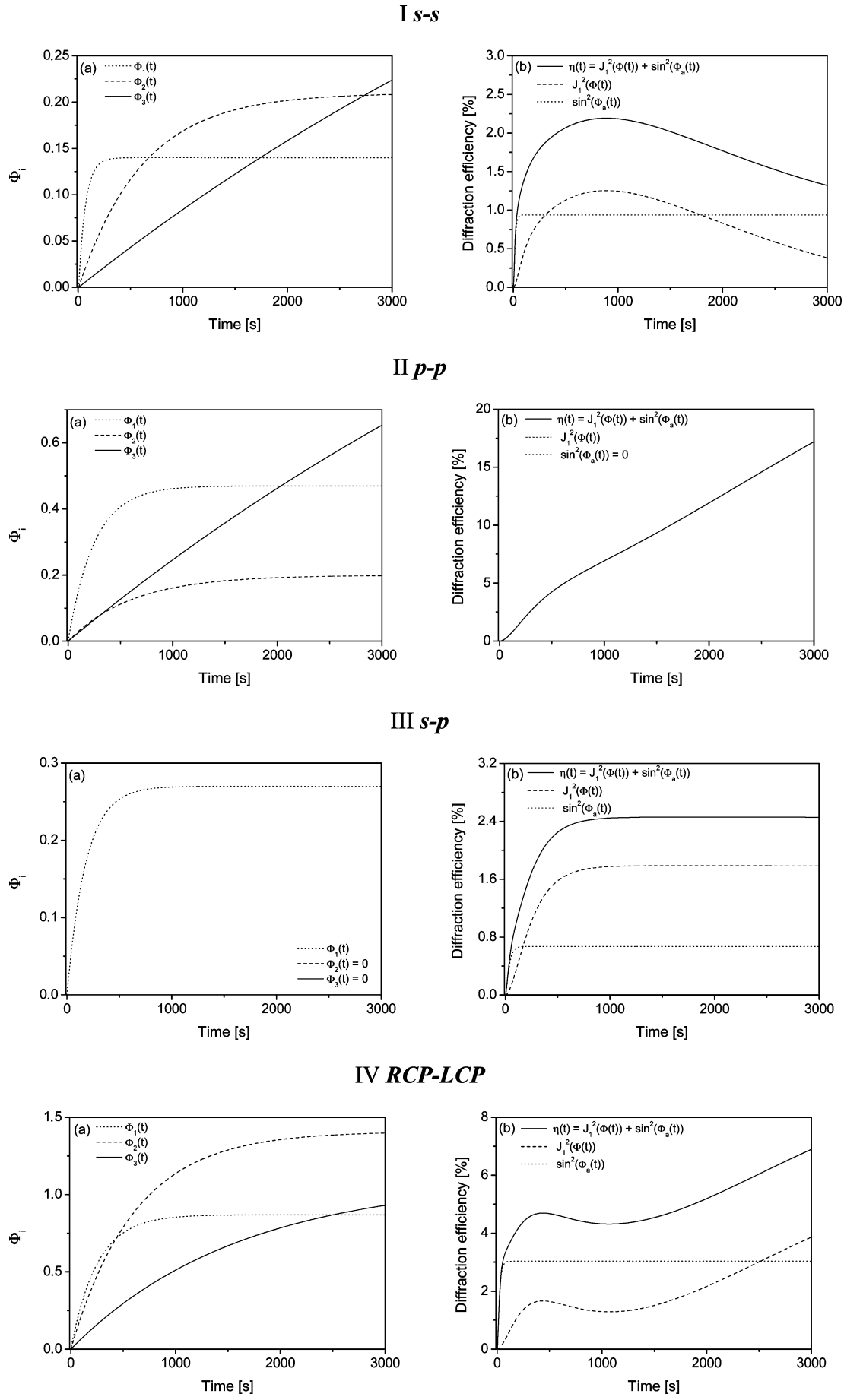

Figure 4. Plots of the dynamics $\Phi(t)$ of individual phase gratings formation (a) and the dynamics of phase grating, the amplitude grating and total diffraction efficiency (b) obtained for *s-s* (I), *p-p* (II), *s-p* (III), and *RCP-LCP* (IV) polarization configurations for RL.

Below we discuss the results of deconvolution of $\eta(t)$ curves for each polarization geometry.

***s-s* Configuration.** The absorption grating and the first phase grating ($\Phi_1(t)$) were responsible for the fast growth of $\eta(t)$ at the beginning of the recording process (cf. Table 3, Figure 4I). After these gratings reached their maximum amplitudes, the second grating ($\Phi_2(t)$), which was formed in-phase to the first grating (Table 3), was still being formed, and its amplitude was increasing, thus the diffraction efficiency increased further until to the end of observation time. At the same time, the third grating ($\Phi_3(t)$), with the significantly higher time constant (Table 3, Figure 4I(a)), was rising, and since it was out-of phase with respect to the $\Phi_1(t)$ and $\Phi_2(t)$, a slow decrease of $\eta(t)$ started to be observed. The slow decrease of the diffraction efficiency was due to slow the build up process of $\Phi_3(t)$. For the longer than established recording time, the minimum could have been observed in $\eta(t)$. The minimum could have appeared when the increasing amplitude of the third grating started to be comparable with the sum of the amplitudes of the first and second gratings that had already reached their maximum amplitudes. After that minimum, a slow increase of the diffraction efficiency could be observed as the result of the still increasing $\Phi_3(t)$.

Fitting parameters revealed that the reorientation grating has the smallest amplitude, while the surface diffusion grating has the highest one. The amplitude of the bulk diffusion grating is only slightly higher than the amplitude of the reorientation grating. Fitting can not reveal the difference in amplitudes of the reorientation $\Phi_{1,max}$ and bulk diffusion $\Phi_{2,max}$ gratings at different wavelengths that is connected with the relatively small refractive index changes in the bulk of a material. However, a significant difference in the $\Phi_{3,max}$ as detected by GL, RL, and IL is observed for the surface diffusion grating. The surface diffusion grating is better seen by GL than RL and IL, which is expected from eq 5. The absorption grating was detected by three wavelengths, and its amplitude $\Phi_{a,max}$ was comparable for $\lambda_1 = 514.5$ nm and for $\lambda_2 = 632.8$ nm and slightly lower for $\lambda_3 = 904$ nm (Table 3).

***p-p* Configuration.** The increase of the diffraction efficiency was due to the build-up of the first and the third grating, which were formed in-phase for *p-p* geometry (Table 3, Figure 4II(a),(b)). The bulk diffusion grating was out of phase to $\Phi_1(t)$ and $\Phi_3(t)$ gratings, and its amplitude $\Phi_{2,max}$ was significantly lower than the sum of the first and third grating amplitudes (Table 3, Figure 4II(a)). Therefore $\Phi_2(t)$ could not have caused the decreasing of $\eta(t)$. In spite of that, the slight influence of bulk diffusion grating on the grating formation process was observed around 500 s as a small inflection in the diffraction efficiency curve (Figure 4II(b), Figure 3b). Further increase of the $\eta(t)$ was the result of the formation of the surface diffusion grating, in which amplitude $\Phi_{3,max}$ was the highest among all studied polarization configurations. Since this grating had significant amplitude, the very high diffraction efficiency close to the theoretical limit was measured for GL. These results are consistent with the previous reports, which unanimously stated that, in the case of the grating formation process in azobenzene-functionalized polymers, the *p-p* polarization configuration is the most effective one for SRG formation.[22,25,27,28,32] Significant surface modulation is, according to the field gradient force model proposed by Tripathy and co-workers, due to the existence of the electric field gradient along the grating wave-vector in *p-p* configuration, which results in efficient mass transport.[25,31,32]

Contrary to the *s-s* polarization case, here the bulk diffusion grating has the smallest amplitude. The surface diffusion grating reveals the highest amplitude, and its value is significantly higher than the amplitudes of the other two gratings. The grating amplitude $\Phi_{3,max}$ is the highest among all studied polarization configuration (cf. Table 3). The detection of the reorientation and bulk diffusion gratings by GL, RL, and IL is comparable (the values of the gratings amplitudes are in the range of error limit), whereas for the surface diffusion grating amplitude $\Phi_{3,max}$ significant differences are observed. The absorption grating was only detected by GL, which is well seen by the rapid small increase in the diffraction efficiency curve at the beginning of the grating recording process (cf. Figure 3b). It was not detected by RL and IL, possibly due to *s*-polarization of these monitoring beams.

***s-p* Configuration.** In this configuration, only the reorientation grating and weak absorption grating were formed (Table 3, Figure 4III(a),(b)). Since only one phase grating is formed, the DEDs will always show clean exponential growth. The amplitude $\Phi_{1,max}$ of the reorientation grating was slightly higher for GL than for RL and IL, and it was comparable for the monitoring beams. It is known that this polarization combination is ineffective in SRG formation, too.[22,27] The grating formation process was relatively fast, and, since there is no bulk and surface diffusion gratings, it is reversible. The reversibility of the grating recording process for *s-p* polarization have already been reported in the literature.[48]

***RCP-LCP* Configuration.** All the phase gratings and the absorption grating were detected by the monitoring wavelengths, whereas the writing wavelength sensed only the surface diffusion grating (Table 3). In this specific grating illumination, the light polarization state along the grating period turns by 180° over the grating period (cf. Table 1). So molecules performing reorientation leading to their perpendicular alignment with respect to the light E-vector at any position make the reorientation and the bulk diffusion gratings invisible for this particular light, but not for any other light inciding on the grating. This is also the reason why the absorption grating was not detected by GL. The DED for RL and IL were completely different from that of GL under the self-diffraction process (cf. Figure 3d). The phase grating Φ_1 and the absorption grating Φ_a are responsible for the fast increase of the diffraction efficiency at the beginning of the recording process for RL (Figures 4IV(a),(b), and 3d) and for IL (Figure 3d). Since $\Phi_2(t)$ and $\Phi_3(t)$ were formed out of phase to $\Phi_1(t)$ (Table 3) and theirs amplitudes increased, a decrease of the diffraction efficiency started to be observed after the maximum. Around 1000 s, the amplitude of the reorientation grating Φ_1 become comparable to the sum of the amplitudes of the bulk and surface diffusion gratings (Figure 4IV(a)); therefore the minimum in $\eta(t)$ was observed. After that, the increase of diffraction was observed again, and it was due to build-up process of the Φ_3 grating, for which amplitude was still growing (Figure 4IV(a)).

The diffraction efficiency obtained for GL was very high due to the meaningful amplitude of the surface diffusion grating and due to not detecting the Φ_1 grating. The diffraction efficiencies measured for RL and IL were significantly lower than that for GL since they detected all three phase gratings, and the Φ_1 grating, having significant amplitude, was formed out-of phase to the Φ_2 and Φ_3 gratings (cf. Table 3).

The amplitudes of the reorientation and the bulk diffusion gratings were (*i*) significant, (*ii*) the highest when compared to the amplitudes of these gratings obtained for other polarization configuration, and (*iii*) comparable to the amplitude of the surface diffusion grating. The absorption grating was only detected by the monitoring wavelengths (its amplitude was higher for RL). The explanation of why the writing beam did not detect the absorption grating has already been given above.

The diffraction grating formation process depends on the polarization configuration of the recording beams. For *s-s*, *p-p*, and *s-p* polarization geometries and when the monitoring beams were linearly polarized, the shapes of the DED curves were similar for all three wavelengths and within each geometry. The difference was observed in the magnitude of $\eta(t)$, which was due to the different detection conditions of these gratings by each wavelength. The shapes of the DED curve were different when the writing and monitoring wavelengths had different polarization states, i.e., circularly and linearly, respectively, as it was in the case of *RCP-LCP* polarization. In other words, the contribution of each grating, the surface diffusion grating in particular, to the total diffraction efficiency depends on the wavelength and on relation between the polarization states of the writing and monitoring beams. The reorientation and the bulk diffusion gratings could not have been detected when the recording beams were circularly polarized. For the same reason, the absorption gratings could not have been monitored in *RCP-LCP* configuration. The absorption grating could not have also been sensed by the *s*-polarized monitoring beam when both writing beams were *p*-polarized.

Generally, the gratings recording time constants were independent of the polarization configuration of the recording beams (the times constants of the bulk diffusion (τ_2), surface diffusion (τ_3), and absorption (τ_a) gratings were identical for *s-s*, *p-p*, and RCL−LCP geometries; cf. Table 3). The difference in the value of the time constants was only observed for the reorientation grating and the absorption grating. In the first case, τ_1 turned out to be the shortest for the *s-s* geometry and the longest for the *p-p* and *RCP-LCP*. It is worth noting that *p-p* and *RCP-LCP* are the most effective for the SRG formation, which can somehow explain the difference in τ_1 between geometries. In the case of the absorption grating time constant, it was slightly longer for *s-p* configuration than for other configurations.

The surface diffusion grating reveals the longest recording time, which seems to be understandable since this grating results from the polymer main chain reorganization and the polymer mass flow expressed as the surface corrugation. Significantly lower recording time is obtained for the bulk diffusion grating.

The significant difference in the diffraction grating formation process for different polarization configurations shows up in the phase shifts between the individual phase gratings, which were completely different for each geometry. In the *s-s* geometry, the surface diffusion grating was out of phase with respect to the reorientation and bulk diffusion gratings. In *p-p* geometry, the bulk diffusion grating was out of phase with respect to the other two phase gratings, while in *RCP-LCP* the reorientation grating was π shifted with respect to the bulk and surface diffusion gratings.

Another quite meaningful difference in the diffraction grating formation process for *s-s*, p-p, and *RCP-LCP* geometries can be noticed in the amplitudes of each phase gratings. Thus, in *s-s* configuration, the smallest amplitude was obtained for the reorientation grating, a larger one was obtained for the bulk diffusion grating, and the largest was obtained for the surface diffusion grating. In the case of *p-p*, the smallest amplitude was measured for the bulk diffusion grating, and the larger was obtained for the reorientation grating, which is contrary to *s-s* geometry. Here also the largest amplitude was obtained for the surface diffusion grating, which, additionally, was the largest among all polarization configurations. For both *s-s* and *p-p* geometries, the strong dominance of the surface diffusion grating was revealed, whereas for *RCP-LCP* configuration, the values of the amplitudes of each gratings were rather comparable, indicating that the grating formation process for *RCP-LCP* is completely different from that for *s-s* and *p-p*. Note that in case of *s-p* geometry, only the refractive index grating is formed, thus the grating formation process in this case is fundamentally different from other configurations.

The above discussion clearly shows that the diffraction grating formation process in azobenzene-functionalized polymers is not a trivial issue.

5. Conclusions

A detailed discussion on the polarization dependence of the holographic grating recording process in azobenzene-functionalized polymer has been presented. Four different polarization combinations of the recording beams: *s-s*, *p-p*, *s-p*, and *RCP-LCP* were used for the grating inscription, and for each of them different DEDs were measured. The grating recording process was simultaneously monitored by three different wavelengths: 514.5 nm (writing) and 632.8 and 904 nm (reading). In order to resolve the experimental DED, a simple model was proposed. The model assumes (*i*) simultaneous formation of three coupling phase gratings during the recording process, (*ii*) fixed in time, equal to 0 or π, phase shifts between phase gratings, and (*iii*) formation of the absorption grating. On the basis of these assumptions, the temporal evolutions of the diffraction efficiency for all polarization configurations and for each wavelengths were precisely fitted. Theoretical results enabled us to make a deep analysis of the diffraction inscription process and allowed for comparison of different polarization geometries used for the grating inscription process. The fundamental difference, beside the different contribution of each grating to the total diffraction efficiency, was the phase shifts between the individual phase gratings, which were different in each geometry. There is no doubt that such a different behavior is caused by particular light-matter interactions and forces acting on molecules from the electric field gradients, light intensity gradients, pressure due to conformational changes in azo-compounds, and temperature gradients. These factors are different for all of the polarization geometries investigated in this work.

Acknowledgment. The authors wish to thank the Ministry of Science and Higher Education (Grant No. NN 507 475237) and the Wroclaw University of Technology for financial support. A.S. is the laureate of The Domestic Grant for Young Scientists awarded by the Foundation for Polish Science.

References and Notes

(1) Hagen, R.; Bieringer, T. Photoaddressable polymers for optical data storage. *Adv. Mater.* **2001**, *13*, 1805–1810.

(2) Viswanathan, N. K.; Kim, D. Y.; Bian, S.; Williams, J.; Liu, W.; Li, L.; Samuelson, L.; Kumar, J.; Tripathy, S. K. Surface relief structures on azo polymer films. *J. Mater. Chem.* **1999**, *9*, 1941–1955.

(3) Harada, K.; Itoh, M.; Umegaki, S.; Yatagai, T.; Kamemaru, S.-I. Application of surface relief hologram using azobenzene containing polymer film. *Opt. Rev.* **2005**, *12*, 130–134.

(4) Blanche, P.-A.; Lemaire, Ph. C.; Maertens, C.; Dubois, P.; Jérôme, R. Polarization holography reveals the nature of the grating in polymers containing azo-dye. *Opt. Commun.* **2000**, *185*, 1–12.

(5) Nikolova, L.; Todorov, T.; Ivanov, M.; Andruzzi, F.; Hvilsted, S.; Ramanujam, P. S. Polarization holographic gratings in side-chain azobenzene polyesters with linear and circular photoanisotropy. *Appl. Opt.* **1996**, *35*, 3835–3840.

(6) Paterson, J.; Natansohn, A.; Rochon, P.; Callender, C. L.; Robitaille, L. Optically inscribed surface relief diffraction gratings on azobenzene-containing polymers for coupling light into slab waveguides. *Appl. Phys. Lett.* **1996**, *69*, 3318–3320.

(7) Rochon, P.; Natansohn, A.; Callender, C. L.; Robitaille, L. Guided mode resonance filters using polymer films. *Appl. Phys. Lett.* **1997**, *71*, 1008–1010.

(8) Natansohn, A.; Rochon, P. Photoinduced motions in azobenzene-based amorphous polymers: possible photonic devices. *Adv. Mater.* **1999**, *11*, 1387–1391.

(9) Rocha, L.; Dumarcher, V.; Denis, Ch.; Raimond, P.; Fiorini, C.; Nunzi, J.-M. Laser emission in periodically modulated polymer films. *J. Appl. Phys.* **2001**, *89*, 3067–3069.

(10) Matsui, T.; Ozaki, M.; Yoshino, K.; Kajzar, F. Fabrication of flexible distributed feedback laser using photoinduced surface relief grating on azo-polymer film as a template. *Jpn. J. Appl. Phys.* **2002**, *41*, L1386–L1388.

(11) Natansohn, A.; Rochon, P. Photoinduced motions in azo-containing polymers. *Chem. Rev.* **2002**, *102*, 4139–4175.

(12) Kang, J.-W.; Kim, M.-J.; Kim, J.-P.; Yoo, S.-J.; Lee, J.-S.; Kim, D. Y.; Kim, J.-J. Polymeric wavelength filters fabricated using holographic surface relief gratings on azobenzene-containing polymer films. *Appl. Phys. Lett.* **2003**, *82*, 3823–3825.

(13) Ubukata, T.; Isoshima, T.; Hara, M. Wavelength-programmable organic distributed-feedback laser based on a photoassisted polymer-migration. *Adv. Mater.* **2005**, *17*, 1630–1633.

(14) Dumont, M.; Sekkat, Z.; Loucif-Säibi, R.; Nakatani, K.; Delaire, J. A. Photoisomerization, photoinduced orientation and orientational relaxation of azo dyes in polymeric films. *Nonlinear Opt.* **1993**, *5*, 395–406.

(15) Dumont, M. A general model for optically induced molecular order in amorphous materials, via photoisomerization. *Nonlinear Opt.* **1996**, *15*, 69–72.

(16) Delaire, J. A.; Nakatani, K. Linear and nonlinear optical properties of photochromic molecules and materials. *Chem. Rev.* **2000**, *100*, 1817–1845.

(17) Rochon, P.; Batalla, E.; Natansohn, A. Optically induced surface gratings on azoaromatic polymer films. *Appl. Phys. Lett.* **1995**, *66*, 136–138.

(18) Kim, D. Y.; Tripathy, S. K.; Li, L.; Kumar, J. Laser-induced holographic surface relief gratings on nonlinear optical polymer films. *Appl. Phys. Lett.* **1995**, *66*, 1166–1168.

(19) Natansohn, A.; Rochon, P. In *Photoreactive Organic Thin Films*; Sekkat, Z., Knoll, W., Eds.; Academic Press: San Diego, CA, 2002; Chapter 13, pp 400−427.

(20) Oliveira Jr., O. N.; Li, L.; Kumar, J.; Tripathy, S. in *Photoreactive Organic Thin Films*; Sekkat, Z., Knoll, W., Eds.; Academic Press: San Diego, CA, 2002; Chap. 14, pp 430−486.

(21) Lagugné-Labarthet, F.; Buffeteau, T.; Sourisseau, C. Analyses of the diffraction efficiencies, birefringence, and surface relief gratings on azobenzene-containing polymer films. *J. Phys. Chem. B* **1998**, *102*, 2654–2662.

(22) Lagugne-Labarthet, F.; Buffeteau, T.; Sourisseau, C. Azopolymer holographic diffraction gratings: time dependent analyses of the diffraction efficiency, birefringence, and surface modulation induced by two linearly polarized interfering beams. *J. Phys. Chem. B* **1999**, *103*, 6690–6699.

(23) Lagugne-Labarthet, F.; Buffeteau, T.; Sourisseau, C. Inscription of holographic gratings using circularly polarized light: Influence of the optical set-up on the birefringence and surface relief grating properties. *Appl. Phys. B: Laser Opt.* **2002**, *74*, 129–137.

(24) Jiang, X. L.; Li, L.; Kumar, J.; Kim, D. Y.; Shivshankar, V.; Tripathy, S. K. Polarization dependent recordings of surface relief gratings on azobenzene containing polymer films. *Appl. Phys. Lett.* **1996**, *68*, 2618–2620.

(25) Tripathy, S. K.; Viswanathan, N. K.; Balasubramanian, S.; Bian, S.; Li, L.; Kumar, J. Polarization dependent holographic write, read and erasure of surface relief grating on azopolymer films. In *Multiphoton and Light Driven Multielectron Processes in Organic: New Phenomena, Materials and Application*; Kajzar, F., Agranovich, M. V., Eds.; NATO Science Series 3; Kluwer Academic Publishers: The Netherlands, Dordrecht/Boston/London, 2000; Vol. 79, pp 421−436.

(26) Bian, S.; Liu, W.; Williams, J.; Samuelson, L.; Kumar, J.; Tripathy, S. K. Photoinduced surface relief grating on amorphous poly(4-phenylazophenol) films. *Chem. Mater.* **2000**, *12*, 1585–1590.

(27) Sobolewska, A.; Miniewicz, A. On the inscription of period and half-period surface relief gratings in azobenzene-functionalized polymers. *J. Phys. Chem. B* **2008**, *112*, 4526–4535.

(28) Audorff, H.; Walker, R.; Kador, L.; Schmidt, H.-W. Polarization dependence of the formation of surface relief gratings in azobenzene-containing molecular glasses. *J. Phys. Chem. B* **2009**, *113*, 3379–3384.

(29) Lagugné-Labarthet, F.; Rochon, P.; Natansohn, A. Polarization analysis of diffracted orders from a birefringence grating recorded on azobenzene containing polymer. *Appl. Phys. Lett.* **1999**, *75*, 1377–1379.

(30) Yager, K. G.; Barrett, Ch. J. All-optical pattering of azo polymer films. *Curr. Opin. Solid State Mater. Sci.* **2001**, *5*, 487–494.

(31) Bian, S.; Williams, J. M.; Kim, D. Y.; Li, L.; Balasubramanian, S.; Kumar, J.; Tripathy, S. K. Photoinduced surface deformations on azobenzene polymer films. *J. Appl. Phys.* **1999**, *86*, 4498–4508.

(32) Kumar, J.; Li, L.; Jiang, X. L.; Kim, D. Y.; Lee, T. S.; Tripathy, S. Gradient force: The mechanism for surface relief grating formation in azobenzene functionalized polymers. *Appl. Phys. Lett.* **1998**, *72*, 2096–2098.

(33) Barrett, C. J.; Natansohn, A. L.; Rochon, P. L. Mechanism of optically inscribed high-efficiency diffraction gratings in azo polymer films. *J. Phys. Chem.* **1996**, *100*, 8836–8842.

(34) Barrett, Ch. J.; Rochon, P.; Natanson, A. Model of laser-driven mass transport in thin films of dye-functionalized polymers. *J. Chem. Phys.* **1998**, *109*, 1505–1516.

(35) Fiorini, C.; Prudhomme, N.; de Veyrac, G.; Maurin, I.; Raimond, P.; Nunzi, J.-M. Molecular migration mechanism for laser induced surface relief grating formation. *Synth. Met.* **2000**, *115*, 121–125.

(36) Lefin, P.; Fiorini, C.; Nunzi, J.-M. Anisotropy of the photoinduced translation diffusion of azo-dyes. *Opt. Mater.* **1998**, *9*, 323–328.

(37) Sumaru, K.; Yamanaka, T.; Fukuda, T.; Matsuda, H. Photoinduced surface relief gratings on azopolymer films: analysis by a fluid mechanics model. *Appl. Phys. Lett.* **1999**, *75*, 1878–1880.

(38) Holme, N. C. R.; Nikolova, L.; Ramanujam, P. S.; Hvilsted, S. An analysis of the anisotropic and topographic gratings in a side-chain liquid crystalline azobenzene polyester. *Appl. Phys. Lett.* **1997**, *70*, 1518–1520.

(39) Reinke, N.; Draude, A.; Fuhrmann, T.; Franke, H.; Lessard, R. A. Electric field assisted holographic recording of surface relief gratings in an azo-glass. *Appl. Phys. B: Laser Opt.* **2004**, *78*, 205–209.

(40) Sobolewska, A.; Miniewicz, A. Analysis of the kinetics of diffraction efficiency during the holographic grating recording in azobenzene functionalized polymers. *J. Phys. Chem. B* **2007**, *111*, 1536–1544.

(41) Sobolewska, A.; Bartkiewicz, S. Three gratings coupling during the holographic grating recording process in azobenzene-functionalized polymer. *Appl. Phys. Lett.* **2008**, *92*, 253305.

(42) Sobolewska, A.; Bartkiewicz, S. On the long time holographic grating recording process in azo-polymer. *Appl. Phys. Lett.* **2009**, *95*, 123302.

(43) Schab-Balcerzak, E.; Sobolewska, A.; Miniewicz, A.; Jurusik, J.; Jarzabek, B. Photoinduced holographic gratings in azobenzene-functionalized poly(amideimides). *Polym. J.* **2007**, *39*, 659–669.

(44) Schab-Balcerzak, E.; Siwy, M.; Kawalec, M.; Sobolewska, A.; Chamera, A.; Miniewicz, A. Synthesis, characterization and study of photoinduced optical anisotropy in polyimides containing side azobenzene units. *J. Phys. Chem. A* **2009**, *113*, 8765–8780.

(45) Henneberg, O.; Geue, Th.; Saphiannikova, M.; Pietsch, U.; Rochon, P.; Natansohn, A. Formation and dynamics of polymer surface relief gratings. *Appl. Sur. Sci.* **2001**, *182*, 272–279.

(46) Schab-Balcerzak, E.; Sobolewska, A.; Miniewicz, A.; Jurusik, J. Chromophore concentration effect on holographic grating formation efficiency in novel azobenzene-functionalized polymers. *Polym. Eng. Sci.* **2008**, *48*, 1755–1767.

(47) Eichler, H. J.; Günter, P.; Pohl, D. W. *Laser-Induced Dynamic Gratings*; Springer-Verlag: Berlin, 1986.

(48) Myśliwiec, J.; Miniewicz, A.; Nespurek, S.; Studenovsky, M.; Sedlakova, Z. Efficient holographic recording in novel azo-containing polymer. *Opt. Mater.* **2007**, *29*, 1756–1762.

JP103756H